Transverse electric field measurements on off-axis n-silicon samples

1998 J. Phys.: Condens. Matter 10 8505

(http://iopscience.iop.org/0953-8984/10/38/011)

J. Phys.: Condens. Matter **10** (1998) 8505–8515. Printed in the UK PII: S0953-8984(98)94377-6

Transverse electric field measurements on off-axis n-silicon samples

S M Zahabi and J E Aubrey

Department of Physics and Astronomy, Cardiff University, PO Box 913, Cardiff CF2 3YB, UK

Received 18 May 1998

Abstract. The anisotropic individual valley mobilities of the conduction band electrons in silicon lead to the formation of space charge regions at the surfaces of a non-(100) layer-shaped sample when a longitudinal electric field is applied. The transverse electric field associated with the redistributed mobile charge has been investigated for n-silicon samples having two off-axis crystallographic orientations. The magnitude of the measured mean transverse electric field was found to be in good agreement with theory, and useful information has been obtained from the measurements on τ_f, the characteristic time for intervalley electron f-scattering in silicon, in the temperature range 77–300 K.

1. Introduction

In an early calculation [1], interest was focused on the dc electrical transport properties of an 'off-axis', i.e. non-(100), layer of n-silicon. A set of coupled differential equations for the excess electron concentrations associated with the three electron valley pairs of the six-valley band structure model was solved, and expressions were found for the transport coefficients of the layer, namely the effective electrical conductivity and the transverse electric field ratio. The value of the former was found to be close to the bulk conductivity of silicon, while the latter is somewhat novel, and is the subject of the present experimental investigation.

Owing to the spheroidal form of the electron constant energy surfaces near the six equivalent conduction band minima of silicon, the mobility of the electrons in a given valley is anisotropic. Therefore when a longitudinal electric field is applied to an off-axis n-silicon layer, a transverse flow of the electrons associated with each valley occurs, leading to significant charge accumulation at the surfaces of the layer. The associated transverse electric field component then gives rise to a transverse voltage across the thickness of the layer. It is convenient to quantify this behaviour by introducing a transport coefficient defined as the ratio of the mean transverse electric field across the layer thickness to the applied longitudinal electric field. Insertion of numerical magnitudes into the expression found for this quantity in [1] indicated that the behaviour described should be observable under attainable experimental conditions.

A simplification made in [1] was to assume that, other than within the space charge regions at the surfaces of the layer, electrical charge neutrality exists at all points. This approximation was replaced in a later calculation [2] by using Poisson's equation. Also by using a mathematically more rigorous approach, a general solution of the problem was found. It was further shown that calculations [1] and [2] gave identical results in the strong

0953-8984/98/388505+11$19.50

screening limit corresponding to large electron concentrations in the layer, but differed for weak screening (see appendix A)†.

Preliminary experimental work carried out on off-axis n-silicon layers having a particular crystallographic orientation proved encouraging [4], and we describe further work here on layers having two different off-axis orientations. The results are found to confirm the predictions of theory, and point to a new transport method of determining the values of characteristic times for electron intervalley scattering processes in semiconductors‡.

2. Experimental details

2.1. Samples

The inset in figure 1 shows schematically the sample geometry assumed in the transport calculations [1] and [2], indicating the direction of the longitudinal applied electric field (along y) and that of the induced transverse electric field (along z). A crystallographic cubic axis labelled $\langle 001 \rangle$ lies in the sample yz plane at an angle ϕ to the direction of the current flowing in the layer, and the $\langle 1\bar{1}0 \rangle$ direction coincides with the sample x axis§. A pair of electrical contacts situated exactly opposite each other on the top and bottom surfaces of the layer would then allow the mean transverse electric field component, $\bar{E}_z$, to be measured‖, and hence the value of the transverse field ratio $\bar{E}_z/E_y$ to be found and compared with theory.

The curve in figure 1 shows the expected form of $\bar{E}_z/E_y$ as a function of the orientation angle ϕ of the silicon layer, based on equation (26) of [1]¶. The ratio has the value zero for layers having $\phi = 0^\circ$, 35.3° and 90°, corresponding respectively to the high symmetry planes (110), (111) and (001). The ratio reverses sign at $\phi = 35.3^\circ$ and passes through extremal values at $\phi \sim 15^\circ$ and $\sim 70^\circ$. Layers having these orientations were selected for the present test of the calculations in [1] and [2].

Figure 2 shows a schematic diagram of the sample configuration adopted for the experimental measurements carried out in the present work. The figure shows a central yz-plane section of an off-axis layer, with a series of four contacts, A, A′, C and C′ on its upper surface and a buried contact B positioned centrally at its lower surface. Standard microelectronic processing techniques were used to fabricate the samples, which, in outline, were as follows. First, p-silicon substrates having the desired crystallographic orientations were phosphorus implanted to yield an n+ buried contact, B, for each sample. Next, n-silicon layers were grown epitaxially on the substrates by VPE*, and the n+ top contacts were then phosphorus implanted. Each sample, occupying a rectangular area, was isolated from its

† Holes were neglected in both calculations [1] and [2], but a further calculation along similar lines with holes included has been completed and has recently been submitted for publication [3]. This work shows that the results derived in [1] and [2] are valid for n-silicon layers having attainable electron concentrations, i.e. they need no correction arising from the neglect of minority holes for such layers.

‡ Parallel work carried out for off-axis GaAs layers has already given useful results [5, 6].

§ This choice of crystallographic orientation was made since two of the three electron groups are then equivalent to each other for transport in the yz plane, thus simplifying the calculation (see appendix A for further details).

‖ The transport calculations give expressions for the position-dependent transverse field component $E_z(z)$ from which $\bar{E}_z$ can readily be calculated.

¶ Rather than presenting a plot of the more general expression (A6) based on [2], with its dependence on the sample electron concentration, the simpler and closely related expression (A5) based on [1] has been plotted in figure 1. The two curves in fact lie close together for the electron concentrations present in the samples measured in our work.

* X-ray diffraction studies confirmed that the VPE-grown layers had the crystallographic orientations of the substrates in each case.

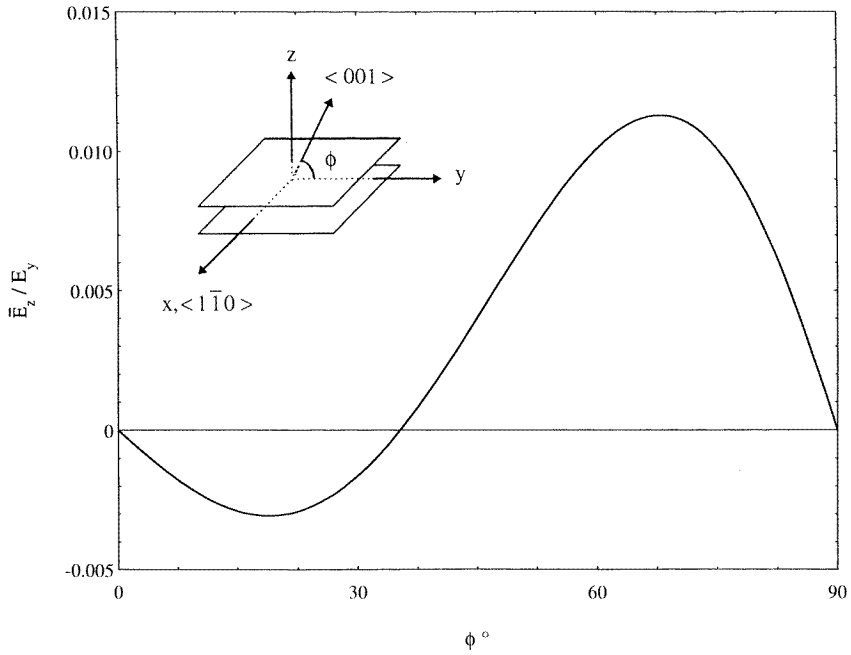

Figure 1. A graph of $\bar{E}_z/E_y$ at 300 K calculated from equation (A5), with $\tau_f = 8.4 \times 10^{-11}$ s, $\mu = 0.13$ m^2 V^{-1} s^{-1}, $r = 5$ and sample thickness $2b = 8$ μm. When equation (A6) is used, with $3N_0 = 5 \times 10^{21}$ m^{-3}, $\bar{E}_z/E_y$ differs by less than 5% from the value shown in the figure at all angles. Inset: layer-shaped sample configuration used in the calculations [1] and [2]. The sample x axis coincides with the $\langle 1\bar{1}0 \rangle$ crystallographic direction, while the $\langle 001 \rangle$ crystal axis is inclined at angle ϕ to the sample y axis. An electric field is applied in the y direction, and the induced transverse field is along the z direction.

surroundings in the VPE-grown layer by boron drive-in around its perimeter. Boron drive-in was also used to isolate a channel through the n-layer to the buried contact B alongside the sample rectangle. The n+ top contacts were Al-metallized, and the free upper surface was then passivated by oxidation. The processed wafers were diced into chips, each holding a pair of samples, and the chips were mounted in dual-in-line packages for protection and ease of handling. The sample contacts were bonded to the package terminals with fine gold wire, and thin glass cover slides were finally cemented in place as further protection for the samples and bonding wires.

Rather than attempting the difficult task of aligning a pair of top and bottom contacts to the sample exactly opposite each other, the bottom contact (i.e. the buried contact B) was positioned as shown, approximately midway between the pair of top contacts A and C: A′ and C′ would then function as current contacts to the device, and the set A, B and C would provide the contacts for the necessary voltage measurements (see appendix B). Approximate sample dimensions and resistivities of the p-substrates and n-layers are given in the caption to figure 2.

2.2. Measurements

Voltage measurements were carried out on the samples in the temperature range 77–300 K, with the sample chips mounted in a variable temperature cryostat. A potential difference

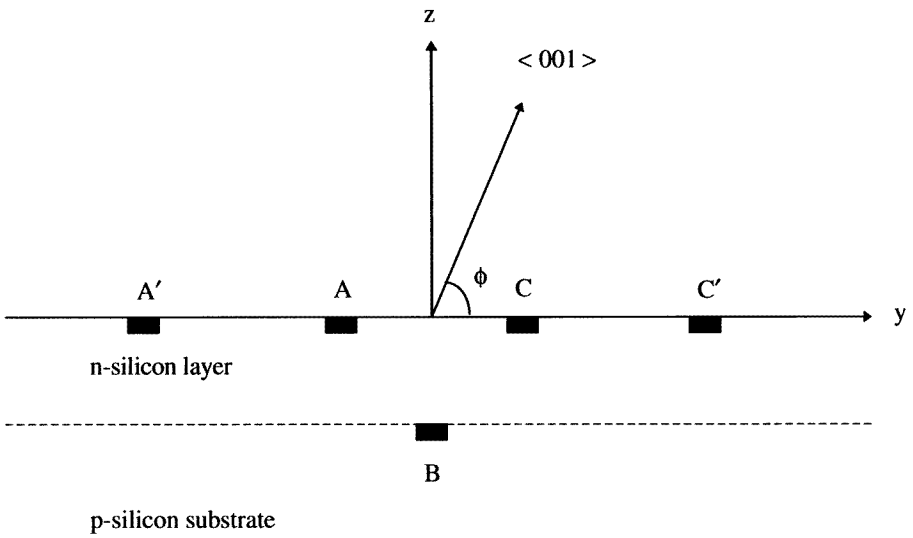

Figure 2. A schematic vertical central section showing the sample geometry. The $\langle 1\bar{1}0\rangle$ crystallographic direction is normal to the plane of the diagram (see the inset in figure 1). The n-silicon layers were ~8 μm thick, the contact intervals on the upper sample surface were ~150 μm and the sample width was ~100 μm. Room temperature resistivity of the n-silicon layers ~0.01 Ω m; room temperature resistivity of the p-silicon substrates ~0.12 Ω m. The orientation angle ϕ had the value 15° for sample 1 and 70° for sample 2.

of order 1 V was applied between the pair of contacts A′ and C′, and the voltages V_{AB} and V_{BC} were measured using a Keithley programmable electrometer, model 617. A PC was programmed to control the experiment, and also to acquire and process the experimental data.

3. Analysis of results

Suppose the sample potential contacts A, B and C in figure 2 have y and z position coordinates $(-a, 0)$, $(0, -2b)$ and $(c, 0)$, taking the origin of coordinates at the upper sample surface. Then the value of the transverse field ratio $\bar{E}_z/E_y$ in the central sample region is as given in the following equation, derived in appendix B,

$$\frac{\bar{V}_{AB} - \bar{V}_{BC}}{\bar{V}_{AB} + \bar{V}_{BC}} = \frac{a-c}{a+c} - \frac{4b}{a+c}\frac{\bar{E}_z}{E_y}. \tag{1}$$

The voltages on the left-hand side of the equation are average values over the two current directions through the layer. The value of the ratio $\bar{E}_z/E_y$ at any temperature can therefore readily be found from these voltages combined with a knowledge of the sample dimensions.

Figures 3 and 4 show plots of $\bar{E}_z/E_y$ against temperature found for sample 1 ($\phi = 15°$) and sample 2 ($\phi = 70°$) respectively. The sign of the ratio is negative for sample 1 and is positive for sample 2, as expected from figure 1.

The transport calculations [1, 2] underlying this work point to the importance of the characteristic time τ_f for electron intervalley f-scattering processes (see appendix A for further details) in determining the magnitude of the transverse field ratio $\bar{E}_z/E_y$. Theoretical expressions for $\bar{E}_z/E_y$ derived in [1] and [2] are given in appendix A. Equation (A5) taken

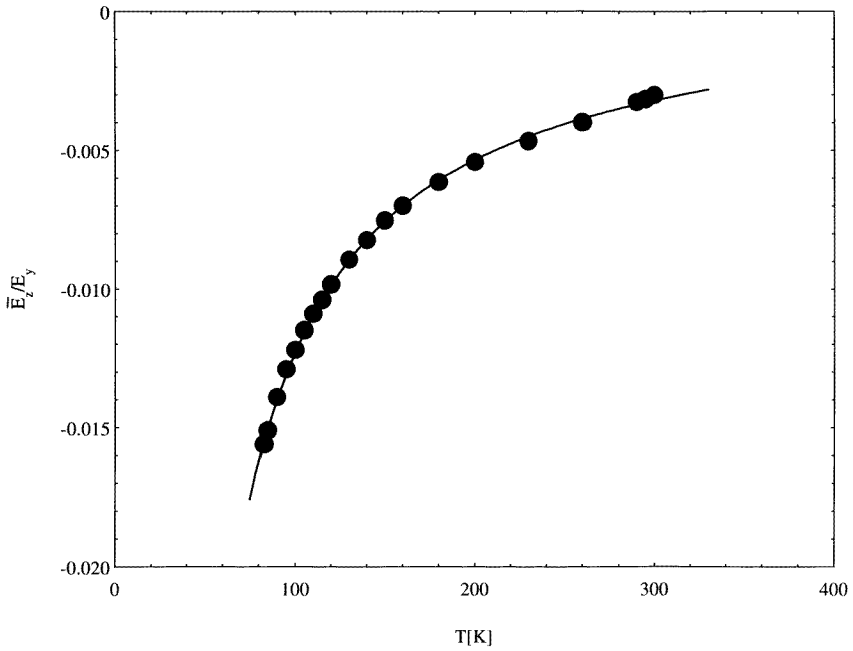

Figure 3. Plot of $\bar{E}_z/E_y$ versus temperature for sample 1 determined as described in the text. For this sample orientation ($\phi = 15^\circ$) $\bar{E}_z/E_y < 0$ as expected from figure 1.

from [1] shows that if the electron mobility as a function of temperature, $\mu(T)$, is known, the experimental $\bar{E}_z/E_y$ data can be reduced immediately to give $\tau_f(T)$. Equation (A6) taken from [2] on the other hand shows that both $\mu(T)$ and the total electron concentration $3N_0(T)$ are needed in order to determine $\tau_f(T)$ from the $\bar{E}_z/E_y$ data. The electron concentrations in the samples investigated were such that the denominator term in square brackets in (A6) was in fact insufficiently small to be neglected, therefore the latter approach was adopted in analysing the $\bar{E}_z/E_y$ data presented here. The $\mu(T)$ and $3N_0(T)$ data used in the calculation are discussed in appendix C. Results for both samples investigated, plotted as $\tau_f(T)$, are given in figure 5.

4. Discussion

Long [7] made a significant advance towards achieving an understanding of the phonon scattering processes which determine the temperature dependence of electron mobility in silicon. He showed that the experimentally determined mobility relaxation time τ_m could be modelled by a certain combination of acoustic and intervalley electron scattering processes. Regarding the latter, guided by the phonon spectrum of silicon [8], he showed that the scattering induced by the complete assembly of intervalley phonons could be adequately represented by contributions from two characteristic phonons, one of low energy and the other of high energy. Expressed as temperatures, Long's characteristic phonon energies were 190 and 630 K.

Long's model has subsequently been refined, with the identification of further characteristic intervalley phonons needed to represent more adequately the scattering induced

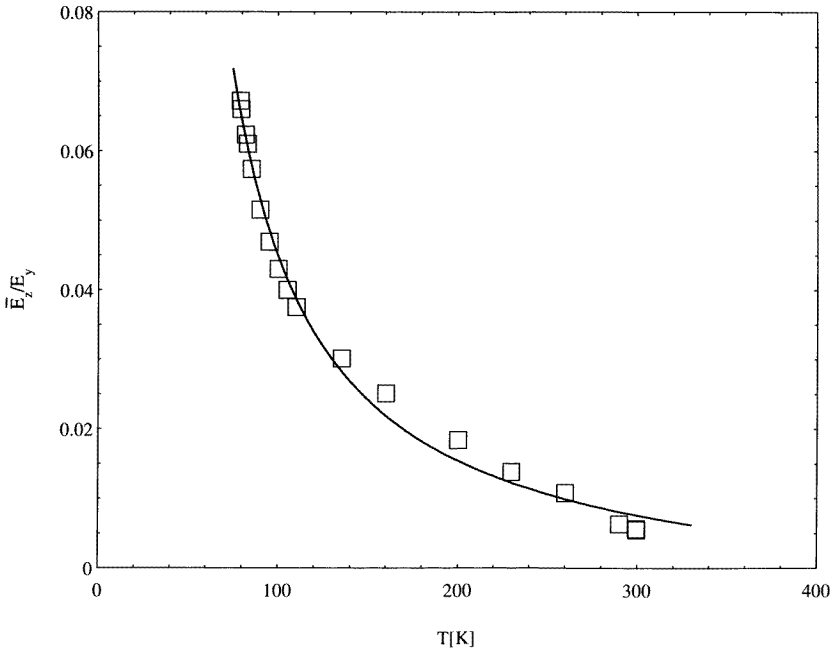

Figure 4. Plot of $\bar{E}_z/E_y$ versus temperature for sample 2 determined as described in the text. For this sample orientation ($\phi = 70^\circ$) $\bar{E}_z/E_y > 0$ as expected from figure 1.

by the entire intervalley phonon assembly. There has also been debate on such matters as the need to describe certain intervalley processes by first order rather than by zero order processes. An excellent review of the subject and related topics has been given by Asche and Sarbei [9].

In the spirit of Long's model, we have adopted the following simple approach in modelling the $\tau_f(T)$ data shown in figure 5. We attribute electron intervalley scattering entirely to a single characteristic phonon of energy θ K (see also an article by Rode [10]), and then expect the f-scattering frequency to be proportional to the number of these phonons present at a given temperature T, i.e. we write

$$\tau_f(T) = A(\mathrm{e}^{(\theta/T)} - 1). \tag{2}$$

The curve through the data points in figure 5 represents equation (2), with $A = 4.4 \pm 0.4 \times 10^{-11}$ s and $\theta = 320 \pm 30$ K.

The preliminary nature of the present work, notably the approximations made which are summarized below, does not warrant attempting to fit the $\tau_f(T)$ data by a physically more realistic intervalley phonon model than the one used here. The θ value we find is intermediate between the values quoted from Long's work, as might be expected, though there is of course little direct physical significance attached to this value in terms of the phonon spectrum of silicon.

It is instructive to compare the magnitude of τ_f found here with that of the relaxation time τ_m determined from electron mobility using the simple formula $\mu = (e/m)\tau_m$. Over the temperature range within which the mobility relaxation time is determined largely by phonon scattering ($T > 100$ K in our samples), τ_f is found to be at least two orders of magnitude larger than τ_m. Even when the multiplicity of equivalent f-scattering processes of

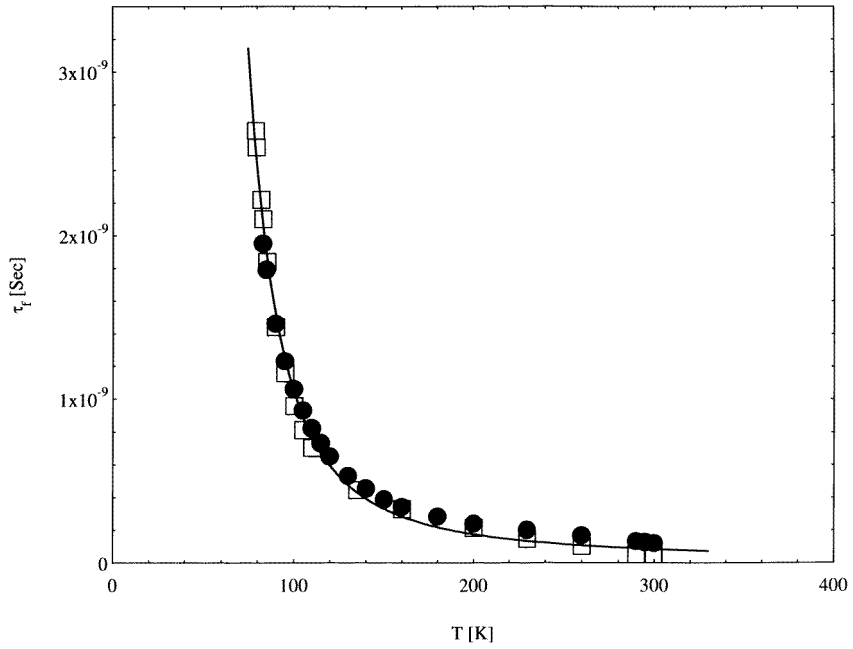

Figure 5. Values of τ_f found from the measurements plotted against temperature: ●, sample 1; □, sample 2. The curve through the points is a plot equation (2) with $A = 4.4 \times 10^{-11}$ s and $\theta = 320$ K.

an electron to other valleys is taken into account, this suggests that intervalley f-scattering contributes relatively weakly to the overall electron scattering frequency in silicon. (See also [4].)

When the data in figure 5 are used to cross check the approximations made in analysing the experimental data (see appendix A), we find a small error only is made by assuming that $\lambda_3 b \gg 1$. Also the inequality $\tau_f \lambda_3 S \ll 1$ assumed in equations (A5) and (A6) implies that the value of the surface intervalley scattering velocity $S < 30$ m s^{-1}. The magnitudes of $\bar{E}_z/E_y$ generally found for the samples investigated here are consistent with the assumption $S = 0$ for both samples (see [4]), justifying the neglect of this term.

The electrical transport calculations underlying the present study were carried out in the linear, low field limit of transport theory. This corresponds to applied fields which are sufficiently small that the excess electron valley-pair populations are very much smaller than their equilibrium population N_0. In this limit ($E_y \leqslant 10^3$ V m^{-1} at the lowest temperature) we expect the transverse field ratio to be independent of applied field E_y: the experimental measurements reported here were made with $E_y \sim 800$ V m^{-1}. Results obtained with fields up to 3×10^3 V m^{-1} showed a degree of field dependence, and this behaviour is being investigated further.

5. Conclusions

We have tested theoretical work on electrical transport effects in off-axis n-silicon layers by carrying out transverse electric field measurements on two off-axis layers having selected crystallographic orientations. Transverse fields have been found in the layers whose

directions and magnitudes accord well with theory. Analysis of the experimental data has yielded values for τ_f, the characteristic time for electron intervalley f processes, which suggest that f scattering is relatively weak in silicon.

The single-phonon model (2) used here clearly has limited physical significance in terms of the actual phonon spectrum of silicon. In future work, with the availability of more precise experimental data and also a transport calculation for a sample representing more exactly the form of the experimental sample, a more precise determination of $\tau_f(T)$ should be possible. This could then be modelled by using a combination of characteristic f-scattering phonons which represents the silicon phonon spectrum more realistically, yielding precise phonon energies and coupling constants [9].

More could be gained from experiments in which both electron mobility and the transverse field ratio are studied simultaneously in a sample. The importance of the transverse field in this context lies in the fact that its value depends exclusively on the f-type intervalley subset of electron scattering processes operating in the crystal. The transverse field measurements therefore offer the opportunity of separating out the contribution of this subset from the totality of scattering processes which together determine the value of the electron mobility in the crystal. The mobility data itself should then yield more precise information on the remaining contributory scattering processes, namely those connected with acoustic and g-type intervalley phonons and processes involving static scattering centres.

Acknowledgments

We wish to thank Professor H A Kemhadjian of Southampton University for supplying the structures studied, and EPSRC for funding the fabrication work. SMZ wishes to acknowledge the award of a postgraduate scholarship by the Government of Iran.

Appendix A. Theoretical expressions for $\bar{E}_z/E_y$

The samples used in this work consisted of off-axis layers whose crystallographic orientations are as shown in the inset in figure 1. Near the silicon conduction band edge, the electron constant energy surfaces in k space consist of pairs of oblate spheroids centred upon the six equivalent energy minima located along ⟨100⟩ type directions [11]. There are therefore three distinct groups of electrons present in silicon, each group being identified by the particular ⟨100⟩ type direction along which its pair of energy minima lies. We label the three groups as follows: group 1 has its pair of minima along ⟨100⟩, group 2 has its minima along ⟨010⟩ and group 3 has its minima along ⟨001⟩.

Owing to the spheroidal shapes of the energy surfaces, electron mobility within a spheroid-pair group is anisotropic, characterized by a second rank tensor with principal values μ_l (longitudinal mobility) and μ_t (transverse mobility) in directions parallel and perpendicular, respectively, to the spheroid rotation axis in each case.

We require the forms of the mobility tensors for each of the three groups present in silicon, referred to the set of sample, x, y and z axes shown in figure 1. The sample crystallographic orientation shown in figure 1 was chosen in the calculations [1] and [2] since this orientation renders electron groups 1 and 2 equivalent to each other for electron motion in the sample yz plane. This leads to a simpler calculation, involving two rather than three non-equivalent groups of electrons. The complete expressions for the required mobility tensors are given in [2], but we need consider only the 2×2 sub-matrices describing yz-plane motion for the two non-equivalent electron groups in our samples. With angle ϕ

as in figure 1, these are as follows:

$$\mu^{(1,2)} = \frac{1}{2}\begin{pmatrix} \mu_l \sin^2\phi + \mu_t(1+\cos^2\phi) & (\mu_t - \mu_l)\sin\phi\cos\phi \\ (\mu_t - \mu_l)\sin\phi\cos\phi & \mu_l\cos^2\phi + \mu_t(1+\sin^2\phi) \end{pmatrix} \quad \text{(A1)}$$

and

$$\mu^{(3)} = \begin{pmatrix} \mu_l\cos^2\phi + \mu_t\sin^2\phi & -(\mu_t - \mu_l)\sin\phi\cos\phi \\ -(\mu_t - \mu_l)\sin\phi\cos\phi & \mu_l\sin^2\phi + \mu_t\cos^2\phi \end{pmatrix}. \quad \text{(A2)}$$

It is convenient at this point to introduce the mean electron mobility $\mu = (2\mu_t + \mu_l)/3$ and the mobility ratio $r = \mu_t/\mu_l$. In terms of these quantities, equation (A1) and (A2) take the form

$$\mu^{(1,2)} = \frac{3\mu}{2(2r+1)}\begin{pmatrix} \sin^2\phi + r(1+\cos^2\phi) & (r-1)\sin\phi\cos\phi \\ (r-1)\sin\phi\cos\phi & \cos^2\phi + r(1+\sin^2\phi) \end{pmatrix} \quad \text{(A3)}$$

and

$$\mu^{(3)} = \frac{3\mu}{2r+1}\begin{pmatrix} \cos^2\phi + r\sin^2\phi & -(r-1)\sin\phi\cos\phi \\ -(r-1)\sin\phi\cos\phi & \sin^2\phi + r\cos^2\phi \end{pmatrix}. \quad \text{(A4)}$$

We now consider the forms of the expressions that were obtained in the calculations [1] and [2] for the transverse field ratio. When the appropriate elements of (A3) and (A4) are substituted into equation (26) of [1], we obtain the result

$$\frac{\bar{E}_z}{E_y} = \left(\frac{\gamma\tau_f\mu}{24}\right)^{\frac{1}{2}} \frac{(r-1)}{b(2r+1)} \sin 2\phi(3\sin^2\phi - 1)[R(\phi)]^{-\frac{1}{2}} \quad \text{(A5)}$$

where

$$R(\phi) = \left(\frac{r+1}{r-1} + \sin^2\phi\right)\left(\frac{r}{r-1} - \sin^2\phi\right).$$

The corresponding result obtained from equation (31) of [2] is as follows:

$$\frac{\bar{E}_z}{E_y} = \left(\frac{\gamma\tau_f\mu}{24}\right)^{\frac{1}{2}} \frac{(r-1)}{b(2r+1)} \sin 2\phi(3\sin^2\phi - 1)[R(\phi)]^{-\frac{1}{2}} \times \frac{1}{1 + [2\varepsilon(2r+1)/9N_0 e\mu\tau_f(r-1)^2 R(\phi)]^{\frac{1}{2}}}. \quad \text{(A6)}$$

The meanings of the symbols in these equations are as follows: $\gamma = kT/e$, τ_f is the electron scattering time for intervalley f processes†, ε the electric permittivity of silicon and $3N_0$ the total conduction electron concentration in the sample.

Two approximations have been made in writing down the expressions (A5) and (A6). First, terms of the form $\tanh\lambda_i b$ ($i = 1, 3$, see [2]), where λ_i^{-1} is a characteristic length present in the problem‡, have been written as unity since $\lambda_i b \gg 1$. Secondly, a term of the form $(1 + \tau_f\lambda_3 S\tanh\lambda_3 b)^{-1}$ appearing in both theoretical expressions has also been written as unity on the grounds that $\tau_f\lambda_3 S \ll 1$, where S is an electron surface intervalley scattering velocity. Both approximations are dealt with briefly in the text.

† In an intervalley f-scattering process, an electron transfers from a valley along one ⟨100⟩ type direction to a second valley, located along another ⟨100⟩ type direction orthogonal to the first. In an intervalley g process, on the other hand, an electron transfers from the initial valley to the other valley located along the same ⟨100⟩ type direction [7]. Whereas f processes alter the electron concentrations in the initial and final groups involved in a transition, g processes simply serve to equalize the concentrations associated with the members of the pair of valleys forming a single group.

‡ Three such characteristic lengths emerge from calculation [2], namely the Debye screening length λ_1^{-1} and two intervalley scattering lengths λ_2^{-1} and λ_3^{-1}. The magnitudes of all three lengths are generally several orders of magnitude smaller than the sample thickness, which justifies the approximation mentioned.

Finally, (A5) and (A6) are strictly valid only for a silicon layer bounded by an insulator at both its surfaces. Whereas the upper surface of our samples had this form, the lower boundary consisted of the pn junction between the n-silicon layer and the p-silicon substrate (see figure 2). We have not taken this into consideration in analysing the experimental results for our samples.

Appendix B. Obtaining experimental values for $\bar{E}_z/E_y$

Equation (1) in the text is derived as follows. Let the potential contacts A, B and C in figure 2 have y and z coordinates $(-a, 0)$, $(0, -2b)$ and $(c, 0)$ respectively. Then suppose initially that a constant field component E_y due to a voltage applied between the sample current contacts A′ and C′ induces a transverse field component $E_z(z)$ in the sample. (See [1] and [2] for the form of $E_z(z)$.) The measured potential differences between the pairs of contacts A, B and B, C are then given by

$$V_{AB} = -aE_y + 2b\bar{E}_z \tag{B1}$$

and

$$V_{BC} = -cE_y - 2b\bar{E}_z \tag{B2}$$

where $\bar{E}_z = (1/2b)\int_{-2b}^{0} E_z(z)\,\mathrm{d}z$, and $2b$ is the sample thickness.
Therefore

$$\frac{V_{AB} - V_{BC}}{V_{AB} + V_{BC}} = \frac{a-c}{a+c} - \frac{4b}{a+c}\frac{\bar{E}_z}{E_y}. \tag{B3}$$

The simple result (B3) is not strictly valid for the samples used in the present work for the following reason. When a voltage is applied between the current

contacts A′ and C′, the previously parallel-sided depletion region between the n-layer and the p-substrate below becomes slightly wedge shaped. What would otherwise have been a uniform applied field E_y in the potential contact region of the sample, as assumed in deriving (B3), is therefore y dependent. A two-dimensional transport simulation [12] indicated that, to a very good approximation, this has the form

$$E_y(y) = E_y(0) - \alpha y. \tag{B4}$$

Here, α is a positive constant, and it can readily be verified that the form of (B4) is not changed on reversing the polarity of the voltage applied to the contacts A′ and C′.

When the above calculation is repeated, but with a constant E_y replaced by the result (B4), we find

$$V_{AB} = -aE_y(0) + 2b\bar{E}_z - \tfrac{1}{2}\alpha a^2 \tag{B5}$$

and

$$V_{BC} = -cE_y(0) - 2b\bar{E}_z + \tfrac{1}{2}\alpha c^2. \tag{B6}$$

If the polarity of the voltage applied to contacts A′ and C′ is now reversed, equations (B5) and (B6) become

$$V_{AB}^{-} = aE_y(0) - 2b\bar{E}_z - \tfrac{1}{2}\alpha a^2 \tag{B7}$$

and

$$V_{BC}^{-} = cE_y(0) + 2b\bar{E}_z + \tfrac{1}{2}\alpha c^2. \tag{B8}$$

We now find that the correction terms in α in equations (B5) to (B8) can readily be eliminated by subtraction, giving the results

$$\bar{V}_{AB} = \frac{V_{AB} - V_{AB}^{-}}{2} = -aE_y(0) + 2b\bar{E}_z \tag{B9}$$

$$\bar{V}_{BC} = \frac{V_{BC} - V_{BC}^{-}}{2} = -cE_y(0) - 2b\bar{E}_z \tag{B10}$$

and

$$\frac{\bar{V}_{AB} - \bar{V}_{BC}}{\bar{V}_{AB} + \bar{V}_{BC}} = \frac{a-c}{a+c} - \frac{4b}{a+c}\frac{\bar{E}_z}{E_y(0)}. \tag{B11}$$

The experimental data were analysed using (B11).

Appendix C. Sample electron concentrations and mobilities

The electrical contacts on the upper surfaces of the samples (see figure 2) were used for four-terminal resistance measurements throughout the work. The room-temperature sample resistivities were used to determine their doping concentrations [13], and the electron concentrations as functions of temperature were then found using a standard equation based upon electrical charge neutrality [14]. Electron mobilities were finally calculated as functions of temperature from the electrical resistivities. Table C1 summarizes the information derived for the two samples investigated.

Table C1.

Sample	ϕ (°)	ρ(300 K) (Ω m)	N_D (10^{21} m^{-3})	μ(300 K) (m^2 V^{-1} s^{-1})	x[a]
1	15	0.0094	5	0.13	1.6_8
2	70	0.0119	4	0.13	1.6_5

[a] Electron mobility in silicon increases with decreasing temperature from 300 K as T^{-x}, before passing through a maximum value somewhat below 100 K [15].

References

[1] Aubrey J E 1981 *J. Phys. C: Solid State Phys.* **14** 1103
[2] Aubrey J E 1988 *Semicond. Sci. Technol.* **3** 902
[3] Evans H B and Aubrey J E 1998 *J. Phys.: Condens. Matter* submitted
[4] Uppal S and Aubrey J E 1995 *Proc. 22nd Int. Conf. on Physics of Semiconductors* ed D J Lockwood (Singapore: World Scientific) p 117
[5] Aubrey J E, Yick G P and Westwood D I 1992 *Electron Lett.* **28** 432
[6] Aubrey J E, Yick G P, Yick P S K and Westwood D I 1992 *Semicond. Sci. Technol.* **7** 861
[7] Long D 1960 *Phys. Rev.* **120** 2024
[8] Brockhouse B N 1959 *Phys. Rev. Lett.* **2** 256
[9] Asche M and Sarbei O G 1981 *Phys. Status Solidi* b **103** 11
[10] Rode D L 1970 *Phys. Status Solidi* b **53** 245
[11] Sze S M 1981 *Physics of Semiconductor Devices* 2nd edn (New York: Wiley) p 14
[12] Evans H B 1998 private communication
[13] Sze S M 1981 *Physics of Semiconductor Devices* 2nd edn (New York: Wiley) p 32
[14] Pierret R F 1987 *Advanced Semiconductor Fundamentals* (Reading, MA: Addison-Wesley) p 128
[15] Sze S M 1981 *Physics of Semiconductor Devices* 2nd edn (New York: Wiley) p 30